ELSEVIER

Atmospheric Research 82 (2006) 416–432

ATMOSPHERIC RESEARCH

www.elsevier.com/locate/atmos

# Effects of stochastic coalescence and air turbulence on the size distribution of cloud droplets☆

Lian-Ping Wang [a,b,*], Yan Xue [a], Orlando Ayala [a], Wojciech W. Grabowski [b]

[a] *Department of Mechanical Engineering, 126 Spencer Laboratory, University of Delaware, Newark, Delaware 19716-3140, USA*
[b] *Mesoscale and Microscale Meteorology Division, National Center for Atmospheric Research, PO Box 3000, Boulder, Colorado 80307-3000, USA*

Accepted 9 December 2005

**Abstract**

An open question in warm rain process and precipitation formation is how rain forms in warm cumulus as rapidly as it has sometimes been observed. In general, the rapid growth of cloud droplets across the size gap from 10 to 50 μm in radius has not been fully explained. Three aspects related to the air turbulence and stochastic coalescence are considered here in an attempt to resolve this open question. The first is the enhanced geometric collision rates caused by air turbulence. The second is the effect of air turbulence on collision efficiencies. The third is stochastic fluctuations and correlations in the collision–coalescence process. Rigorous approaches are developed to address these issues. Preliminary results indicate that turbulence could shorten the time for drizzle formation to about a half of the time needed for the same growth process based on hydrodynamic–gravitational mechanism alone. To address the effect of stochastic correlations, we derive and validate a true stochastic coalescence equation. It is hoped that this new mean field equation will be useful in the future to improve the deterministic kinetic collection equation.


*Keywords:* Cloud microphysics; Turbulence; Geometric collision rate; Collision efficiency; Stochastic coalescence

## 1. Introduction

Cloud droplets of radii less than 10 to 15 μm grow efficiently through diffusion of water vapor, and droplets larger than 30 to 50 μm in radii grow efficiently through gravitational collisions (Langmuir, 1948; Kogan, 1993; Beard and Ochs, 1993; Pruppacher and Klett, 1997). An open question is why rain forms in warm (i.e., ice-free) cumulus clouds as rapidly as it has sometimes been observed. Radar observations in tropical regions show that rain can form in cumulus clouds by warm rain process in approximately 15 to 20 min (Szumowski et al., 1997; Knight et al., 2002).[1]

☆ Submitted to Atmospheric Research on January 31, 2005. Revised version submitted on June 15, 2005.

* Corresponding author. Department of Mechanical Engineering, 126 Spencer Laboratory, University of Delaware, Newark, Delaware 19716-3140, USA. Tel.: +1 302 831 8160; fax: +1 302 831 3619.
*E-mail address:* lwang@udel.edu (L.-P. Wang).

0169-8095/$ - see front matter © 2006 Elsevier B.V. All rights reserved.
doi:10.1016/j.atmosres.2005.12.011

[1] This time is typically defined as the time interval for radar reflectivity to evolve from about −20 dBZ to at least 20 dBZ, roughly corresponding to 10 μm and 250 μm average droplet sizes in radius, respectively, for a liquid water content at 0.5 g/m$^3$. However, as noted by Knight et al. (2002), it is difficult to define precisely the starting time and ending time for rain initiation in radar observations, as the radar reflectivity depends on both the average droplet size and the liquid water content. For this reason, only a very few published observational studies reported this time interval.

This 20-min time interval is also quoted in Rogers and Yau (1989, p. 121) as the average time for the initiation of warm rainfall (i.e., from the initial development of a cumulus cloud to the first appearance of rain). Theoretical predictions based on the gravitational-coalescence mechanism alone would require a time interval on the order of an hour for droplets to grow from 20 to 100 μm in radius (the actual time depends on the initial droplet size spectrum in clouds, see Pruppacher and Klett, 1997) Therefore, there appears to be a factor of 2 or more difference between the predicted growth time and the observed growth time. In general, it is difficult to explain the rapid growth of cloud droplets in the size range from 10 to 50 μm in radius (i.e., the so-called size gap) for which neither the condensation nor the collision–coalescence mechanism is very effective. The onset of drizzle-size (~100 μm in radius) raindrops is still poorly understood in many precipitating cloud systems. A related issue is the discrepancy between the width of measured and simulated size distributions of cloud droplets. In particular, the question why measured droplet size distributions are in general broader is not fully understood (Beard and Ochs, 1993; Khain et al., 2000; Brenguier and Chaumat, 2001; Chaumat and Brenguier, 2001).

Several mechanisms have been considered in the past to explain the rapid development of rain in shallow convective clouds (Beard and Ochs, 1993; Pruppacher and Klett, 1997; Khain et al., 2000). The first mechanism involves entrainment of dry environmental air into the cloud. Although entrainment lowers the cloud water content (and thus has a negative impact on rain development), it can result in dramatic impact on cloud droplet spectra. In particular, broad spectra are typically produced as a result of entrainment and mixing (Brenguier and Grabowski, 1993; Su et al., 1998). The second mechanism involves effects of giant aerosol particles which allow formation of large cloud droplets (Johnson, 1982). Srivastava (1989) suggested that the droplet spectral width can be broadened by considering local values of the water vapor supersaturation rather than the mean supersaturation that a large population of cloud droplets experience. However, recent numerical results by Vaillancourt et al. (2001, 2002) suggest that this effect contributes insignificantly to the width of the cloud droplet spectrum. The fourth mechanism concerns effects of air turbulence on the relative motion of droplets, concentration fluctuations, and collision efficiencies (Khain et al., 2000; Franklin et al., 2005;Wang et al., 2005b). Finally, in addition to the above physical mechanisms, the commonly used kinetic collection equation for modeling the time evolution of droplet size distribution is not fully consistent with the stochastic nature of the collision–coalescence process (Telford, 1955; Scott, 1967; Gillespie, 1972, 1975a).

This paper concerns the effects of air turbulence and stochastic coalescence. A brief overview of recent advances towards quantifying the effects of air turbulence on collision rate and collision efficiency will be presented. The impact of enhanced geometric collision rate by turbulence on droplet size distribution will be illustrated by Monte-Carlo simulations. The role of stochastic coalescence will be explicitly revealed by a rigorously derived, true stochastic coalescence equation (TSCE) which contains correlations of droplet numbers in different sizes. We shall validate the TSCE using Monte-Carlo simulations and the analytical result of Bayewitz et al. (1974). The level and nature of stochastic correlations and fluctuations will also be discussed.

## 2. Effects of air turbulence

Over the last 10 years, several studies have been published in both engineering and atmospheric literature concerning the collision rate of particles in a turbulent flow. These studies suggest, at least qualitatively, that the enhancement of the collision–coalescence mechanism associated with the cloud turbulence might be a likely explanation for the rapid growth of cloud droplets across the size gap. These recent advances are based mostly on numerical simulations and qualitative theoretical arguments, indicating that the collection kernel of cloud droplets can be enhanced by several effects of turbulence, including (1) enhanced relative motion due to differential acceleration and shear effects (Kruis and Kusters, 1997; Pinsky and Khain, 1997; Sundaram and Collins, 1997; Wang et al., 2000; Zhou et al., 2001; Dodin and Elperin, 2002); (2) enhanced average pair density due to local preferential concentration of droplets (Sundaram and Collins, 1997; Wang et al., 2000; Zhou et al., 2001; Zaichik and Alipchenkov, 2003; Zaichik et al., 2003); (3) enhancement due to selective alterations of the settling rate by turbulence (Wang and Maxey, 1993; Davila and Hunt, 2001; Ghosh and Jonas, 2001), and (4) enhanced collision efficiency (Koziol and Leighton, 1996; Pinsky et al., 1999, 2000; Wang et al., 2005b). The levels of enhancement depend, in a complex manner, on the size of droplets (which in turn determines the response time and settling velocity) and the strength of air turbulence (i.e., the dissipation rate, Reynolds number, etc.).

While all the studies consistently point to collision enhancements by air turbulence, they should be viewed

as qualitative results as far as the collision–coalescence of cloud droplets is concerned. This is because the context and the approximations used in most of these studies do not match the conditions of cloud droplets, e.g., see discussions in Grabowski and Vaillancourt (1999) and Vaillancourt and Yau (2000). Also, the levels of enhancement concluded from different studies are vastly different. This status is related to the complexity of the collisional interactions in a turbulent flow, and the lack and inaccuracy of direct measurements of turbulence and droplet distribution in clouds. Recent observations and analyses of observational data from the Fast FSSP probe suggest some evidence that clouds droplets inside adiabatic cores may not be distributed randomly in space, but the conclusions have not been consistent and the issue remains largely unresolved (Chaumat and Brenguier, 1998; Jameson and Kostinski, 2000; Kostinski and Shaw, 2001; Pinsky and Khain, 2002). For a more elaborated discussion of observational studies on the spatial distribution of cloud droplets, the readers are referred to Section 3 of Grabowski and Vaillancourt (1999). In a wind tunnel setting, Vohl et al. (1999) reported that turbulence could lead to a 10% to 20% increase in the overall collision kernel when the flow dissipation rate was in the range of 110 to 690 $cm^2/s^3$. Due to the different regions in the parameter space that different studies tend to address (Vaillancourt and Yau, 2000), the extent and dominant lengthscale associated with clustering of cloud droplets and turbulence effects are still an open question. Although with these limitations, the recent studies do contribute to a major progress in the understanding and kinematic formulation of collection kernel for droplets with and without hydrodynamic interactions (Sundaram and Collins, 1997; Wang et al., 1998, 2000; Zhou et al., 2001; Wang et al., 2005b), which will be useful in the future for the parameterization of collection kernel of cloud droplets.

### 2.1. Impact of enhanced geometric collision rate

Although with the above limitations, a major progress has been made in the understanding and kinematic formulation of collection kernel (Sundaram and Collins, 1997; Wang et al., 2000; Zhou et al., 2001). The average geometrical collision kernel between two arbitrary droplet size groups can be described *kinematically* as (Sundaram and Collins, 1997; Wang et al., 1998, 2000)

$$c_{12} = 2\pi R^2 < |w_r(\text{No HI})| > g_{12}(\text{No HI}). \quad (1)$$

where the geometric collision radius $R$ is the sum of the radii of two colliding droplets, $R = a_1 + a_2$, $w_r$ is the radial relative velocity, the abbreviation "No HI" denotes statistics computed without considering the disturbance flows due to droplets, $g_{12}$ is the radial distribution function measuring the effect of preferential concentration on the pair number density at separation $r$. By geometric collisions, these kinematic properties are computed without considering droplet–droplet hydrodynamic interactions. Air turbulence can increase $w_r$ due to local fluid acceleration and shear effects (Saffman and Turner, 1956; Wang et al., 1998). Furthermore, when the inertial response time of droplets is on the order of the flow Kolmogorov time scale, droplets could respond effectively to the dynamics of small-scale flow structures and become nonuniformly distributed, a phenomenon known as the preferential concentration (Maxey, 1987; Squires and Eaton, 1990; Wang and Maxey, 1993). Since the average collision rates are related to the second moment of the droplet concentration, the preferential concentration can cause $g_{12}$ to be greater than one (Sundaram and Collins, 1997; Wang et al., 2000) and thus significantly increases the collision kernel.

To gain a quantitative understanding of how the enhanced geometric collision rates by turbulence may promote to growth of cloud droplets, the following idealized but *exact* calculation using discrete mass classes was performed. Consider a system, say about 1 $cm^3$ volume, initially containing 60 droplets of 20 μm in diameter and another 60 droplets of 22 μm in diameter. These two droplet sizes were placed in bin 3 and bin 4 as two discrete sizes since their mass ratio is very close to 4/3, as such bin 1 and bin 2 were unoccupied in the full discrete mass representation involving a total of 420 bins. The elemental mass (the mass for bin 1) is taken to be 1/3 of the mass of a 20-μm droplet. If all these droplets were to coalesce to form a single droplet, the final droplet size would be 103.8 μm in diameter and would belong to the mass bin 420 (i.e., $420 = 60 \times 3 + 60 \times 4$).

A fully stochastic collision–coalescence calculation was carried out using the Monte-Carlo method of Gillespie (1975b). The Monte-Carlo method, although computationally more expensive, inherently incorporates all stochastic correlations (see Section 3 below for further details) and also eliminates the numerical errors in solving the kinetic collection equation (Bott, 1998; Tzivion et al., 1999; Simmel et al., 2002). Eq. (1) was used to parameterize the collision kernel with the model of $<|w_r|>$ after Wang et al. (1998) and $g_{12}$ taken from Zhou et al. (2001). The parameterization of $g_{12}$ in Zhou et al. (2001) was developed based on direct numerical simulations (DNS) at low flow Reynolds numbers but was extrapolated to high flow Reynolds numbers. This

extrapolation was done using established Reynolds-number scaling rules for local fluid shear rates and for the ratio of large to small scales in high Reynolds-number turbulence (Hinze, 1975). Stokes drag was assumed and the collision efficiency was set to unity. 10,000 Monte-Carlo realizations were used to obtain the average droplet size distribution and related statistics. The rms fluctuation velocity $u'$ of the air turbulence was assumed to be 1 m/s in order to derive the Taylor microscale Reynolds number which was given as $R_\lambda = u^2\sqrt{15/v\varepsilon}$, where $v$ is air kinematic viscosity and $\epsilon$ is the flow dissipation rate.

In Fig. 1 we show time evolution of the average numbers in three separate bins, namely, from top to bottom, corresponding to 20, 60, and 103.8 μm in diameter, respectively. Three levels of flow dissipation were considered and the results were compared to the base case of no air turbulence. Statistical uncertainties, an inherent feature of Monte-Carlo simulations, were also shown. The time was normalized by the characteristic time scale $T$ of the gravitational coagulation process ($T$=2891 s). The average number for 20-μm droplets decreases monotonically due to collision–coalescence events; however, the rate of depletion depends on the flow dissipation rate. The higher the flow dissipation, the faster the depletion rate.

While for the intermediate sizes (Fig. 1(b)), the mean number first increases with time (the production phase), reaches a peak value at a critical time, and then decreases afterwards (the depletion phase). The production phase and the critical time occur earlier as the flow dissipation rate is increased. The peak value is also less for larger flow dissipation rate due to a faster spreading of the size spectrum. Finally the depletion phase happens earlier and is completed faster as the flow dissipation rate increases. All of these imply an enhanced growth of cloud droplets due to effects of turbulence.

The average number for the last bin increases monotonically as expected (Fig. 1(c)). One can see that turbulence can shorten the time for the largest droplet to form. For the case of $\epsilon$=400 cm$^2$/s$^3$,the time for the coalescence process to complete is roughly half of that for the pure gravitational case.

To better quantify how turbulence promote the growth of droplets, we computed the droplet diameter based on the mean droplet mass and show its time evolution in Fig. 2. Clearly, the droplets grow faster as the flow dissipation rate is increased. We show in Table 1 the time in seconds for the droplet diameter based on mean mass to reach a certain size. At high flow dissipation rate, turbulence may shorten the growth time

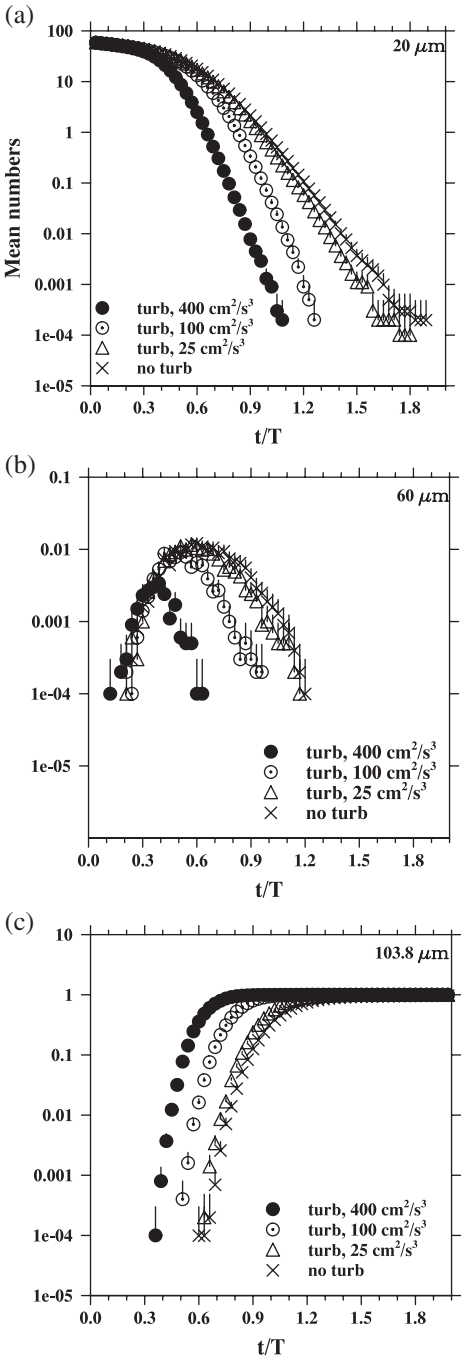


Fig. 1. The time evolution of average number in (a) bin 3 (20 μm in diameter), (b) bin 81 (60 μm in diameter), and (c) bin 420 (103.8 μm in diameter).

by as much as 30% to 40%. This clearly shows that turbulence can speed up the growth of cloud droplets.

The main open issue here is the modeling of the radial distribution function $g_{12}$ at high flow Reynolds numbers and how the radial distribution function is

affected by the gravitational settling, as the relative velocity, $w_r$, can be more easily modelled. Theoretical advances in this direction are currently being made (Jeffery, 2001; Sigurgeirsson and Stuart, 2002; Zaichik and Alipchenkov, 2003; Zaichik et al., 2003). DNS and experimental data at higher flow Reynolds are certainly desired as well. The recent DNS studies by Franklin et al. (2005) and Wang et al. (2005b) represent efforts to obtain quality simulation data relevant to cloud droplets.

### 2.2. Collision efficiencies

For droplets of radii less than 60 μm, hydrodynamic interactions between two colliding droplets can significantly affect the trajectories of the droplets due to short inertial response time and small settling rate. It follows that the collision efficiency is a sensitive function of droplet sizes (Klett and Davis, 1973;Wang et al., 2005). While there have been a large number of studies on the collision efficiency due to the gravitational–hydrodynamic interaction of two isolated cloud droplets (Pruppacher and Klett, 1997), only a very few studies exist in the literature concerning collision efficiencies of cloud droplets in turbulent air (de Almeida, 1979; Grover and Pruppacher, 1985; Jonas, 1996; Koziol and Leighton, 1996; Pinsky et al., 1999, 2000; Wang et al., 2005b). A careful review of these studies reveals that *different* kinematic formulations were used to define the collision efficiency, almost all of which are some extensions to the definition based on grazing trajectory, which is only strictly valid for the gravitational–hydrodynamic interaction of two isolated cloud droplets (Wang et al., 2005b). Furthermore, these kinematic definitions of collision efficiency were used in these studies without *direct* validation using dynamic collision statistics. This problem along with various (often) inaccurate representations of the air turbulence and different droplet-size combinations has generated somewhat controversial conclusions regarding the influence of turbulence on collision efficiencies.

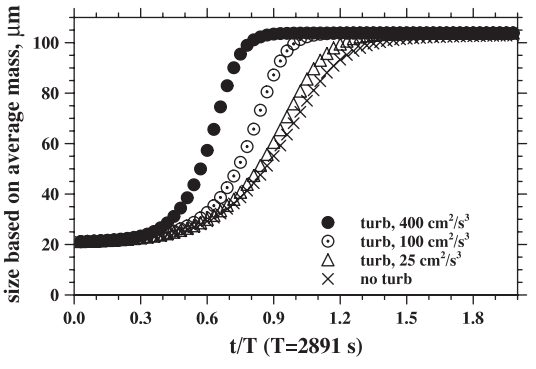


Fig. 2. Diameter in micrometers based on the average droplet mass as a function of time.

Table 1
Time in seconds for the droplet diameter based on mean mass to reach a certain size

| $\epsilon$(cm$^2$/s$^3$) | 40 μm | 60 μm | 90 μm |
|---|---|---|---|
| 0 | 2208 | 2703 | 3354 |
| 25 | 2148, 97% | 2594, 96% | 3131, 93% |
| 100 | 1938, 88% | 2270, 84% | 2646, 79% |
| 400 | 1500, 68% | 1763, 65% | 2081, 62% |

The percentages are obtained by dividing the times by the corresponding value for the gravitational case.

Therefore, the topic of collision efficiency of cloud droplets in a *turbulent suspension* is widely open. Recently we have successfully developed a hybrid direct numerical simulation (HDNS) approach (Wang et al., 2005b) to allow an accurate evaluation of the effect of turbulence on collision efficiency. The HDNS approach combines a pseudospectral simulation of air turbulence with an improved superposition method (Wang et al., 2005a) for the disturbance flows due to droplets. This approach allows, for the first time, the direct incorporation of hydrodynamic interactions within DNS and computations from first principles of all statistical information related to collision–coalescence.

Our main findings to date are summarized here. First we have demonstrated that the same kinematic formulation, Eq. (1), can be used to describe the collision kernel of hydrodynamically interacting droplets, namely,

$$C_{12} = 2\pi R^2 < |w_r(\mathrm{HI})| > g_{12}(\mathrm{HI}) = 2\pi R^2 < |w_r(\mathrm{No\ HI})| > g_{12}(\mathrm{No\ HI}) E_{12}, \quad (2)$$

but now the kinematic properties $w_r$ and $g_{12}$ are computed with droplet–droplet hydrodynamic interactions considered. Here "HI" indicates statistics computed with hydrodynamic interactions included in the simulations, namely, droplets move under the influence of disturbance flows due to all other droplets, in addition to the drag force due to the background flow, gravity, and inertia (Wang et al., 2005b). On the other hand, the abbreviation "No HI" denotes statistics computed without considering the disturbance flows due to droplets. Computations of kinematic properties require finite corrections due to the fact that droplets can no longer overlap in space (Wang et al., 2005b). The true collision efficiency $E_{12}$ is defined as

$$E_{12} = \frac{< |w_r| > (\mathrm{HI})}{< |w_r| > (\mathrm{No\ HI})} \times \frac{g_{12}(\mathrm{HI})}{g_{12}(\mathrm{No\ HI})}. \quad (3)$$

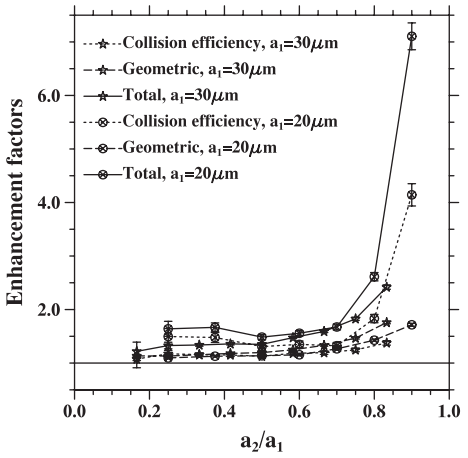


Fig. 3. Enhancement factors due to the turbulence measured relative to the results of the gravitational–hydrodynamic case for $a_1=20$ and 30 μm as a function of $a_2/a_1$ ($\epsilon$=400 cm$^2$/s$^3$). The total enhancement factor is the enhancement factor on geometric kernel times the enhancement factor on collision efficiency.

This kinematic formulation then separates the effect of turbulence on collision efficiency from the enhanced geometric collision rate.

Fig. 3 shows enhancement factors due to turbulence measured relative to the results of the gravitational–hydrodynamic case, when the flow dissipation rate is 400 cm$^2$/s$^3$. Air turbulence increases both the geometric collision rate and the collision efficiency, particularly when collisional interactions between similar-size droplets ($a_2/a_1\rightarrow 1$) are considered. For $a_1=30$ μm, the enhancement factor on the geometric collision rate is larger than the enhancement factor on collision efficiency. However, when $a_1=20$ μm, the enhancement factor on the collision efficiency is much greater that that of the geometric collision rate. In other words, the effect of air turbulence on the collision efficiency depends sensitively on the size of the larger droplets. Furthermore, both the effects of turbulence on the collision efficiency and the geometric collision rate depend on the level of flow dissipation rate. We observe that hydrodynamic interactions are less effective in changing the relative radial velocity in a turbulent flow, when compared to the pure hydrodynamic–gravitational problem. This is the main reason that turbulence enhances the collision efficiency, in addition to augment the geometric collision rate. We also find that hydrodynamic interactions increase the near-field pair density, resulting in higher radial distribution function at contact when compared to the geometric collision case. The overall enhancement factor on collision kernel by turbulence can be as large as 2 to 6 when the flow dissipation rate is high.

Furthermore, the collision efficiency for collisions among equal-size droplets depends on the presence of the other size droplets in a binary suspension, due to the cumulative weak far-field hydrodynamic interactions of all droplets in the suspension (Wang et al., submitted for publication). This observation implies that the collision efficiency based on the interaction of two isolated droplets, as is often theoretically treated in the past, may not be applicable to a suspension of many droplets, even for the hydrodynamic–gravitational problem.

Much work is needed to understand and quantify the effect of turbulence on collision efficiency. We are in the process of conducting a parametric study of collision efficiency for different droplet-pair sizes, different flow dissipation rates, and Reynolds numbers. The goal will be to develop a parameterization model to quantify the enhanced collision efficiency by air turbulence which can later be used to study its impact on the size evolution of cloud droplets.

## 3. Stochastic coalescence

Typically, the modeling of size distribution in a collision–coalescence system is performed by a mean-field equation such as the classical Smoluchowski coagulation equation (Smoluchowski, 1917),

$$\frac{\mathrm{d}N_m}{\mathrm{d}t}=\frac{1}{2}\sum_{k=1}^{m-1}C_{k,m-k}N_kN_{m-k}-N_m\sum_{k=1}^{\infty}C_{m,k}N_k \tag{4}$$

where $N_m$ is the average number of droplets of mass equal to $m$ elemental mass units, per unit volume at time $t$. $C_{m,k}$ is the collision kernel between $m$-size droplets and $k$-size droplets. Here we only consider the discrete formulation as in Gillespie (1972). The first term on the right hand side represents rate of generation of $m$-size droplets due to all coalescence events of pairs of small droplets with the sum of their masses equal to that of $m$-size droplet. The second term on the right hand side is the rate of depletion due to all coalescence events involving $m$-size droplets. Such *deterministic* Smoluchowski equation or kinetic collection equation (KCE) describes how the number density of a certain mass evolves in time. Although the term "stochastic" has been associated with the above equation for historical

Table 2
Analogy between coalescence modeling and fluid mechanics

| Level of approach | Coalescence models | Fluid mechanics |
|---|---|---|
| Particle-level | Monte-Carlo method (e.g., Gillespie, 1975b) | Molecular dynamics |
| Phase space | State space probability (e.g., Sec. 2 of Bayewitz et al., 1974) | Boltzmann equation |
| Field variables | P (*n, m; t*) (e.g., Gillespie, 1972) | Navier–Strokes eqn |
| Full moment eqns | *Not fully known* (e.g., Sec. 3 of Bayewitz et al., 1974) | Full Reynolds-averaged Navier–Strokes (RANS) eqn |
| Modeled moment eqns | Example: Smoluchowski equation (Smoluchowski, 1917) | Modeled RANS eqns |

reasons to imply that a full spectrum of different droplet sizes are considered, the above equation is clearly deterministic and has no stochastic correlations or fluctuations included.

Telford (1955), in his pioneering work on stochastic coalescence, first introduced the probabilistic interpretation to the occurrence of instantaneous coalescence events assuming that (1) the concentration of the droplets available for collection remains unchanged during their removal by coalescences and (2) the collecting drops do not interact among themselves. The possibility of having a range of sizes for the collecting drops greatly increases the spectral width of the drops than in the earlier continuous growth model in which all collecting drops are assumed to be of the same size. Recently, Kostinski and Shaw (2005) published a simplified version of Telford's analysis to illustrate that stochastic fluctuations can lead to a factor-of-10 acceleration in the growth of a few lucky drops. However, the descriptions of Telford (1955) and Kostinski and Shaw (2005) are stochastically rather incomplete. In general, coalescence events occur randomly and its local rates vary in space, time, and with realizations, the size distribution modeling must consider the stochastic nature of the coagulation process. The stochastic completeness of the kinetic collection equation was later studied by Scott (1967), Warshaw (1967), Long (1971), Gillespie (1972, 1975a), Bayewitz et al. (1974). The common wisdom is that when the system volume or number of droplets is very large, the stochastic fluctuations tend to be small compared to the mean values. However, we may argue that, when a particular droplet size class is considered, the number may not always be large simply due to the system initial condition. Spatial inhomogeneity and fluctuations can also be augmented by air turbulence, which adds another dimension to the stochastic nature of the coalescence process.

Here we shall revisit the question of stochastic completeness in coalescence modeling. Table 2 provides an overview of all the different approaches that have been developed to model size distribution of droplets in a collision–coalescence system, and draws an analogy between these approaches and different approaches used to describe fluid flow. From top to bottom in Table 2, the degrees of freedom of the system are systematically reduced while the nature of governing rules or equations changes from linear to nonlinear. Of importance is that the full moment equations for a coalescence system have not been derived in general, except for the special case of constant collision kernel by Bayewitz et al. (1974). We will show below how to derive the full mean field equation at the first order which we will refer to as the true stochastic coalescence equation (TSCE). Full mean field equations at higher order could be similarly derived. We will then point out an error in the derivation of Bayewitz et al. (1974), namely, Eq. (6) of their paper.

### 3.1. The master equation or the V-equation

We shall follow the approach of Bayewitz et al. (1974, hereafter BYKS74) by specifying the state of a realization of the system at any time by the numbers of droplets for all possible discrete mass (or size) groups, $x_1, x_2, x_3, \ldots, x_{N_0}$. The total number of droplets is denoted by $N$, namely, $N=\sum x_k$.

Let $M_1$ be the mass of the elemental droplets. The mass of the $k$-th size group is assumed to be given as $M_k=k\,M_1$. For any given realization, the mass conservation states

$$\sum_k M_k x_k = M_1 \sum_k k x_k = M_1 N_0, \tag{5}$$

where $N_0$ is the largest possible mass class. The system would be completely specified by the probability distribution $v(N, x_1, x_2, x_3, \ldots; t)$ of the state space $(N, x_1, x_2, x_3, \ldots)$ and, by definition, the summation of over the state space is unity:

$$\sum_{x_1}\sum_{x_2}\cdots\sum\sum_{x_{N_0}} v(N, x_1, x_2, x_3 \ldots; t) = 1 \tag{6}$$

It is assumed that the coalescence kernels $C_{j,k}$; $j,k=1, 2,\ldots, N_0$, have been determined such that $C_{j,k}\mathrm{d}t$ represents the probability that a given pair of cloud droplets with masses $M_j$ and $M_k$ will coalesce in the next infinitesimal time interval d$t$ (Gillespie, 1972; Bayewitz et al., 1974; Gillespie, 1975a,b). $C_{j,k}$ may be a function of $M_j$ and $M_k$, but we shall assume $C_{j,k}$ does not depend on $x_j$ and $x_k$, a reasonable assumption as long as the total volume concentration of droplets is very small and only binary collisions need to be considered.

To develop a governing equation for $v(N, x_1, x_2, x_3\ldots; t)$, we follow the arguments of BYKS74 and examine three sets of scenarios, during the infinitesimal time interval from $t\rightarrow t+\mathrm{d}t$, that will contribute to $v(N, x_1, x_2, x_3\ldots; t+\mathrm{d}t)$: (1) a coalescence takes place between two droplets of the same size; (2) a coalescence occurs between two droplets of different sizes; and (3) no coalescence occurs. The first contribution requires consideration of all neighboring states ($N+1, x_1, \ldots, x_k+2,\ldots, x_{2k}-1, \ldots$) at time $t$ and, after summing over all different pairs and droplets sizes, is given as

$$\sum_k v(N+1, x_1, \ldots, x_k+2, \ldots, x_{2k}-1, \ldots; t)\binom{x_m+2}{2}C_{k,k}\mathrm{d}t.$$

The second contribution requires consideration of all neighboring states ($N+1, x_1, \ldots, x_j+1, \ldots x_k+1, \ldots, x_{j+1}-1, \ldots$) at time $t$ and is

$$\underbrace{\sum_j\sum_k}_{j<k} v(N+1, x_1, \ldots, x_j+1, \ldots, x_k+1, \ldots, x_{j+k}-1, \ldots; t)(x_j+1)(x_k+1)C_{j,k}\mathrm{d}t.$$

The last contribution should be

$$v(N, x_1, x_2, x_3\ldots; t)\left[1-\underbrace{\sum_j\sum_k}_{j<k} x_j x_k C_{j,k}\mathrm{d}t-\sum_k\binom{x_k}{2}C_{k,k}\mathrm{d}t\right].$$

The sum of these three contributions will be equal to $v(N, x_1, x_2, x_3\ldots; t)$, therefore, the governing equation for $v(N, x_1, x_2, x_3\ldots; t)$ can be written as

$$\begin{aligned}\frac{\mathrm{d}}{\mathrm{d}t}v(N, x_1, x_2, x_3, \ldots; t) =& \underbrace{\sum_j\sum_k}_{j<k} v(N+1, x_1, \ldots, x_j+1, \ldots, x_k+1, \ldots, x_{j+k}-1, \ldots; t)\times(x_j+1)(x_k+1)C_{j,k}\\ &+\sum_k v(N+1, x_1, \ldots, x_k+2, \ldots, x_{2k}-1, \ldots; t)\binom{x_k+2}{2}C_{k,k}\\ &-v(N, x_1, x_2, x_3, \ldots; t)\left[\underbrace{\sum_j\sum_k}_{j<k} x_j x_k C_{j,k}+\sum_k\binom{x_k}{2}C_{k,k}\right].\end{aligned} \tag{7}$$

We shall call the above equation the master equation or V-equation. The above equation extends the formulation of BYKS74 for the special case of constant coalescence kernel to arbitrary collision kernels. The above description is stochastically complete. Once the probabilities of the states are determined, one can derive all other statistical quantities. The probability distribution for a given particle mass can be written as:

$$P(n, m; t) = \sum_{\text{All but } x_m} v(N, x_1, x_2, \ldots, x_m = n, \ldots; t), \tag{8}$$

where the summation is understood as over all the state variables except $x_m$.

The mean and moments of particle number for a given mass are

$$< x_m > \equiv \sum_{\text{All}} x_m v, \qquad < x_m^n > \equiv \sum_{\text{All}} x_m^n v; \tag{9}$$

where the summation is over the full state space. Likewise, correlations can also be evaluated as

$$< x_j x_k > \equiv \sum_{\text{All}} x_j x_k v. \tag{10}$$

Here the brackets imply an average over all realizations in the state space. We shall define the cross-correlations coefficient $\rho_{jk}$ as

$$\rho_{jk} = \frac{< x_j x_k > - < x_j >< x_k >}{\sqrt{(< x_j^2 > - < x_j >^2)(< x_k^2 > - < x_k >^2)}}. \tag{11}$$

Of particular importance is the fact that the system of equations represented by Eq. (7) are linear and can, in principle, be *solved analytically* for *arbitrary* variable collision kernels, in terms of eigenvalues and eigenvectors of the linear system. Furthermore, random initial conditions can be handled by a probability-weighted superposition of deterministic initial conditions because of the linearity. The analytical solutions can be used to validate numerical solutions such as those based on Monte-Carlo method (Gillespie, 1975b) and to study the correlations between different particle sizes (BYKS74). Of course, in practice, this is only feasible for a system containing a small number of droplets since the total number of states increases extremely quickly with $N_0$. For example, the total number of states for $N_0$=5, 10, 40, and 100 are 7; 42; 37,338; and 190,569,292; respectively.[2]

### 3.2. Derivation of the true stochastic coalescence equation (TSCE)

We shall now present a derivation for the true stochastic collision–coalescence equations. While BYKS74 presented such an equation for the special case of constant collision kernel, no derivation was given in their paper. Therefore, this section serves two purposes: (1) to present a detailed derivation and (2) to show that it is possible to develop the true stochastic coalescence equations for arbitrary collision kernels. To our knowledge, this has not been attempted in terms of discrete masses, although some discussions in terms of continuous mass are provided by Ramkrishna and co-workers (Ramkrishna and Borwanker, 1973, 1974; Ramkrishna et al., 1976).

Multiplying Eq. (7) by $x_m$ and then summing over all state space, we have

$$\begin{aligned}\frac{\mathrm{d} < x_m >}{\mathrm{d}t} = & \underbrace{\sum_{\text{All}} \sum_{\text{k}} v(N+1,\ldots,x_k+2,\ldots,x_{2k}-1,\ldots;t)\frac{(x_k+2)(x_k+1)}{2} x_m C_{k,k}}_{\text{A}} \\ & + \underbrace{\sum_{\text{All}} \underbrace{\sum_{\text{j}} \sum_{\text{k}}}_{j<k} v(N+1,\ldots,x_j+1,\ldots,x_k+1,\ldots,x_{j+k}-1,\ldots;t)(x_j+1)(x_k+1) x_m C_{j,k}}_{\text{B}} \\ & \underbrace{- \sum_{\text{All}} \underbrace{\sum_{\text{j}} \sum_{\text{k}}}_{j<k} v(N,x_1,x_2,x_3,\ldots;t) x_j x_k x_m C_{j,k}}_{\text{C}} - \underbrace{\sum_{\text{All}} \sum_{\text{k}} v(N,x_1,x_2,x_3,\ldots;t)\frac{x_k(x_k+1)}{2} x_m C_{k,k}}_{\text{D}}.\end{aligned} \tag{12}$$

The range of values that $k$ may take in term $A$ is from 1 to $\mathrm{int}\left(\frac{N_0}{2}\right)$, where

$$\mathrm{int}\left(\frac{N_0}{2}\right) \equiv \begin{cases} N_0/2, & \text{if } N_0 \text{ is even} \\ (N_0-1)/2, & \text{if } N_0 \text{ is odd.} \end{cases} \tag{13}$$

[2] Finding all distinct states for a given total number is known as the partition problem, see for example, (Andrews, 1998).

Rewriting Term $A$ in Eq. (12) as

$$A = \sum_{\text{All}} \sum_{k} (\cdot) = \sum_{k} \sum_{\text{All}} (\cdot) = \underbrace{\sum_{k}}_{k\neq m/2, k\neq m} \sum_{\text{All}} (\cdot) + \gamma(m) \sum_{\text{All}} (\cdot)_{k=m/2} + \omega(m) \sum_{\text{All}} (\cdot)_{k=m}, \tag{14}$$

where we have introduced the notation, following Gillespie (1972), that

$$\gamma(m) \equiv \begin{cases} 1, & \text{if } m \text{ is even} \\ 0, & \text{if } m \text{ is odd.} \end{cases} \tag{15}$$

The second notation $\omega(m)$ is defined as

$$\omega(m) \equiv \begin{cases} 1, & \text{if } m \leq \text{int}\left(\frac{N_0}{2}\right) \\ 0, & \text{if } m > \text{int}\left(\frac{N_0}{2}\right). \end{cases} \tag{16}$$

Noting the state location of the probability $v$, the three parts of the term $A$ then become

$$\begin{aligned} A = & \underbrace{\sum_{k}}_{k\neq m/2,\ k\neq m} \frac{1}{2} < x_k(x_k-1)x_m > C_{k,k} + \frac{\gamma(m)}{2} < x_{m/2}(x_{m/2}-1)(x_m+1) > C_{m/2,m/2} + \frac{\omega(m)}{2} \\ & < x_m(x_m-1)(x_m-2) > C_{m,m} = \sum_{k} \frac{1}{2} < x_k(x_k-1)x_m > C_{k,k} + \frac{\gamma(m)}{2} < x_{m/2}(x_{m/2}-1) > C_{m/2,m/2} - \omega(m) \\ & < x_m(x_m-1) > C_{m,m} \end{aligned} \tag{17}$$

Similarly, the second term $B$ can be handled as

$$\begin{aligned} B = & \underbrace{\sum_{j}\sum_{k}}_{j<k, j+k\leq m-1} \sum_{\text{All}} (\cdot) + \underbrace{\sum_{j}\sum_{k}}_{j<k, j+k=m} \sum_{\text{All}} (\cdot) + \underbrace{\sum_{j}\sum_{k}}_{j<k, j+k\geq m+1, j\neq m, k\neq m} \sum_{\text{All}} (\cdot) + \underbrace{\sum_{j}\sum_{k}}_{j<k, j+k\geq m+1, j\neq m, k\neq m} \sum_{\text{All}} (\cdot) \\ & + \underbrace{\sum_{j}\sum_{k}}_{j<k, j+k\geq m+1, j\neq m, k\neq m} \sum_{\text{All}} (\cdot) \\ = & \underbrace{\sum_{j}\sum_{k}}_{\text{Part 1: } j<k, j+k\leq m-1} C_{j,k} < x_m, x_j x_k > + \underbrace{\sum_{j}\sum_{k}}_{\text{Part 2: } j<k, j+k=m} C_{j,k} < (x_m+1)x_j x_k > \\ & + \underbrace{\sum_{j}\sum_{k}}_{\text{Part 3: } j<k, j+k\geq m+1, j\neq m, k\neq m} C_{j,k} < x_m, x_j x_k > + \underbrace{\sum_{j}}_{\text{Part 4: } j<m} C_{j,m} < (x_m-1)x_j x_m > \\ & + \underbrace{\sum_{k}}_{\text{Part 5: } k>m} C_{m,k} < (x_m-1)x_m x_k > . \end{aligned} \tag{18}$$

It is crucial to understand all the possible combinations of $j$ and $k$ as represented by the five parts in term $B$. In Fig. 4, we show all these combinations by different symbols and indicate the sub-domains covered by the five parts shown on the right hand side of Eq. (18). Note that the last term in Eq. (18) would not be there if $m > \text{int}\left(\frac{N_0}{2}\right)$ since $j+k \leq N_0$ (see Fig. 4). However, it is harmless to drop the constraint $j+k \leq N_0$ and to let the domain extend over all the region covered by $k>j$ with $k \leq N_0$ and $j \leq (N_0-1)$. This is because the extended region makes zero contribution anyway since

$$< (\ldots)x_j x_k > = 0, \text{ if } j+k > N_0.$$

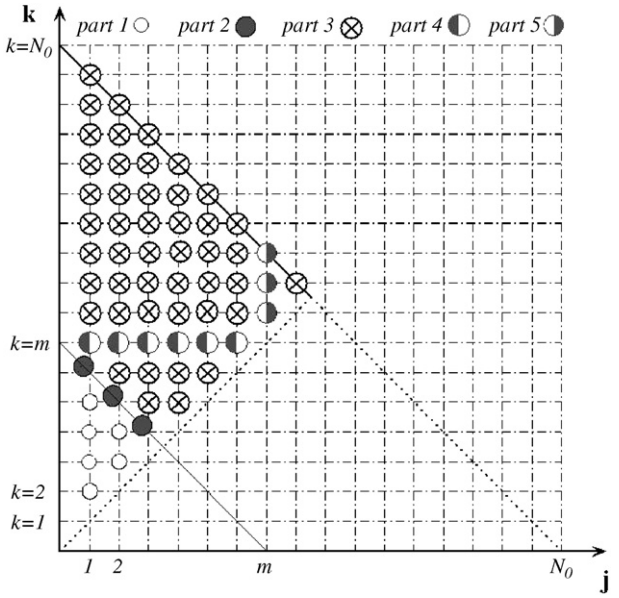


Fig. 4. The five sub-domains covered by the five parts in term $B$, as displayed in the order shown in Eq. (18).

Namely, when $j+k>N_0$, $x_j$ and $x_k$ cannot take non-zero value simultaneously because of the constraint of the total system mass. This same concept may be applied to the other terms in Eq. (18), and that is why we did not explicitly state $j+k\le N_0$ in the summations. However, this domain extension must be taken with care when (i) the last two terms in Eq. (18) are combined, as given in the next expression; (ii) any nonzero terms involving $j=k>\mathrm{int}(N_0/2)$ must be excluded from the final equations.

Eq. (18) can be rearranged to obtain

$$B=\underbrace{\sum_j\sum_k}_{j<k} C_{j,k}<x_m x_j x_k>+\underbrace{\sum_j\sum_k}_{j<k,\ j+k=m} C_{j,k}<x_j x_k>-\sum_k C_{k,m}<x_k x_m>+\omega(m)C_{m,m}<x_m^2> \tag{19}$$

The reason for including $\omega(m)$ in the last term has been stated in the last paragraph. The key to the above steps is to recognize that, when $j$ or $k$ overlaps with $m/2$, $m$, or $2m$, the terms must be handled with care.

The last two terms in Eq. (12) reduce to

$$C=\underbrace{\sum_j\sum_k}_{j<k} C_{j,k}<x_m x_j x_k> \tag{20}$$

$$D=\sum_k C_{k,k}\frac{1}{2}<x_m x_k(x_k-1)> \tag{21}$$

Substituting Eqs. (17), (19)–(21) into Eq. (12) and noting that

$$\underbrace{\sum_j\sum_k}_{j<k,\ j+k=m} C_{j,k}<x_j x_k>=\frac{1}{2}\sum_{k=1}^{m-1}C_{k,m-k}<x_k x_{m-k}>-\frac{\gamma(m)}{2}C_{m/2,m/2}<x_{m/2}^2>.$$

we obtain finally

$$\frac{\mathrm{d}<x_m>}{\mathrm{d}t} = \underbrace{\frac{1}{2}\sum_{k=1}^{m-1} C_{k,m-k} < x_k x_{m-k} >}_{\text{Term } A} \underbrace{- \sum_{k=1}^{N_0-m} C_{m,k} < x_m x_k >}_{\text{Term } B} \underbrace{+\omega(m) C_{m,m} < x_m >}_{\text{Term } C} \underbrace{- \frac{\gamma(m)}{2} C_{m/2,m/2} < x_{m/2} >}_{\text{Term } D} \tag{22}$$

This is the true stochastic coalescence equation (TSCE).

### 3.3. Results and discussion

Eq. (22) is almost identical to Eq. (6) in BYKS74 when all $C_{j,k}$ are set to one. However, there are two important differences between our equation and the equation given in BYKS74. First, the range for $k$ in the second term on the right hand side is here explicitly specified. The upper bound $k=N_0-m$ is necessary to exclude any unphysical coagulations between two particles with the sum of their mass larger than the total mass of the system. This is a very important requirement and must be satisfied at each individual realization.

Secondly, the third term on the right hand side is zero here when $m>\mathrm{int}(N_0/2)$, because of $\omega(m)$. We can show easily that $\omega(m)$ is necessary because of the mass conservation

$$\frac{\mathrm{d}}{\mathrm{d}t}\sum_{m=1}^{N_0} m < x_m >= 0. \tag{23}$$

Without $\omega(m)$, Eq. (22) would not satisfy Eq. (23), since the first two terms on the right hand side of Eq. (22) would cancel each other if the operation $\sum_{m=1}^{N_0} m(..)$ is taken. Therefore, Eq. (6) in BYKS74 is not correct because $\omega(m)$ is missing.

The third term (Term $C$) on the right-hand-side of Eq. (22) is a correction to Term $B$ required to reinstate the correct bookkeeping of the number of pairs for self-collisions. The forth term is a correction to term $A$ for the same reason. These correction terms are not relevant if self-collisions are not involved such as the case of gravitational collision–coalescence.

Unlike the usual, deterministic KCE, the TSCE, Eq. (22), contains correlations among instantaneous droplets of different sizes. In Fig. 5, we display the value of all terms in the TSCE for the case of $C_{i,j}=1$ with $N_0=100$ and $m=80$, using the analytical solution of BYKS74. Initially, it is assumed that $x_m=N_0\delta_{m1}$. This figure demonstrates that the left hand side of TSCE and the right hand side of TSCE are exactly the same. We can also conclude that the additional term $C$ and term $D$ in TSCE can be important for large droplet sizes or for later times. Using the analytical solution of BYKS74, we can obtain correlation coefficients of droplet number fluctuations for different mass pairs for the case of

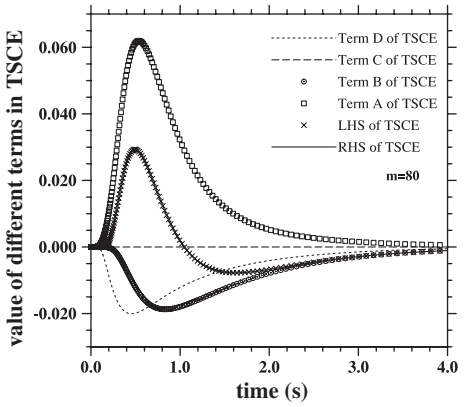


Fig. 5. Validation of the TSCE for the case of constant collision kernel when applied to 80. The initial system size is equal to 100.

constant collision kernel. The analytical solution of BYKS74 involves subtractions of extremely large numbers in a series summation, and care was taken to make sure that the final result is correct. Monte-Carlo simulations were also used to check the results. Fig. 6(a) shows results for 1–2 and 2–3 pairs for two different system sizes $N_0$. When plotted against $N_0t$, the results overlap for two system sizes. The magnitude of correlation coefficients can be quite large. $\rho_{1,2}$ is close to −1 at small times for the reason that, given the initial condition, only self collisions between size-1 droplets are possible and these generate only size-2 droplets initially. $\rho_{2,3}$ is almost always negative because the only way size-3 droplets are produced is through coalescences of size-2 droplets with size-1 droplets. Therefore, the production of size-3 droplets goes with the depletion of size-2 droplets. The negative value of $\rho_{2,3}$ will impact the production rate of size-5 droplets. Also shown in Fig. 6(b) is the ratio of rms fluctuation to the mean for three different droplet sizes and two system sizes. We can see that the rms fluctuations may be much larger than the mean if the mean is small. For an initially narrow size distribution, the mean values in large size bins are all necessarily small.

The non-zero correlations and large relative fluctuations shown above would imply that the size distribution may not be correctly modelled by the usual KCE in general. Consider a system initially containing 100 monodisperse elemental droplets and $C_{i,j}=1$. If all droplets coalesce, the final state is one large droplet of 100 times the elemental mass. We compare, in Fig. 7, results of mass distribution using three different approaches: the stochastically complete approach of BYKS74, KCE, and the truncated KCE (i.e., Eq. (4) with only 100 bins considered). Fig. 7 shows that the mass distribution is almost the same for the three approaches at early time $t=0.1$. At later time ($t=0.6$), however, they give different results. The difference is partly due to the fluctuation correlations discussed above. The truncation at $m=N_0=100$ also accelerates the production of the largest droplet when compared to the untruncated KCE.

Finally, we note that the nature of collision kernel can affect the level of the correlation coefficients. Fig. 8 compares results obtained by Monte-Carlo simulations, for gravitational collision kernel and a turbulent collision kernel at

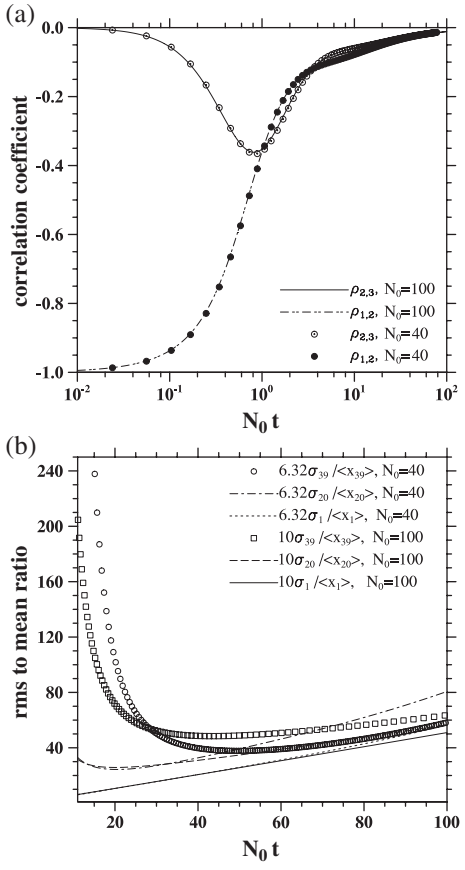


Fig. 6. (a)Analytical correlation coefficients and (b) ratio of rms fluctuation to the mean for the case of constant collision kernel.

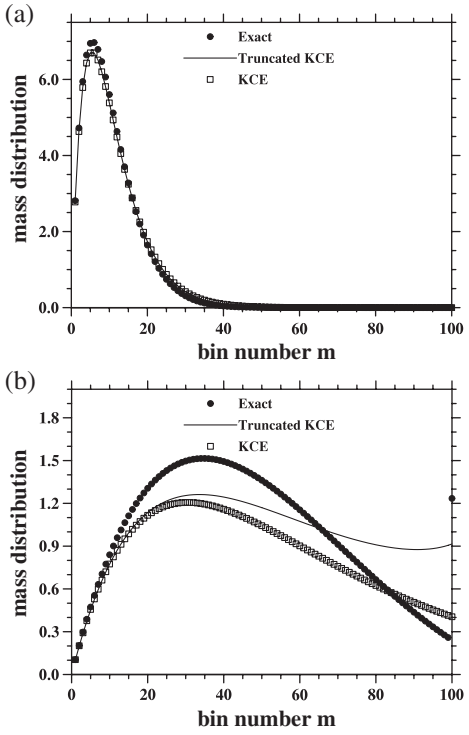


Fig. 7. Mass distribution obtained from different approaches: (a) $t=0.1$; (b) $t=0.6$.

$\epsilon=100\ \mathrm{cm}^2/\mathrm{s}^3$. These kernels and the initial conditions are the same as these used in Section 2.1. Of importance is that the turbulent collision kernel results in larger correlation coefficients, implying that the deviation from the KCE description due to the stochastic coalescence is larger in a turbulent flow. We also compared the mass distributions obtained from the Monte-Carlo method with that obtained by solving the truncated KCE. Fig. 9 displays the distributions at $t=T$ for two of the cases discussed in Section 2.1. The difference between the two is indeed larger for the turbulent kernel case, particularly at later times.

Our ultimate goal is to use TSCE to identify the conditions under which the usual deterministic collision–coalescence mean-field equation such as KCE can be applied, or else how the mean field equation could be improved to account for the stochastic nature of the coalescence process. Our strategy for future research developments is to use the

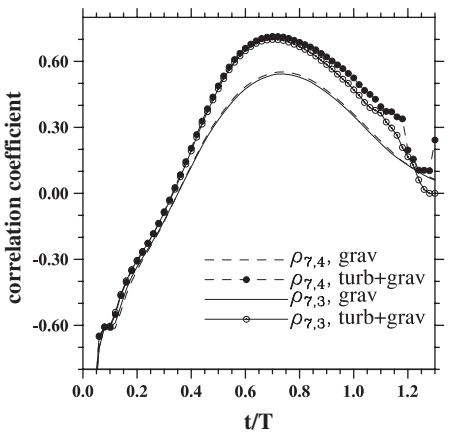


Fig. 8. Correlation coefficients for hydrodynamic kernels with and without air turbulence. The time scale $T=2891$ s.

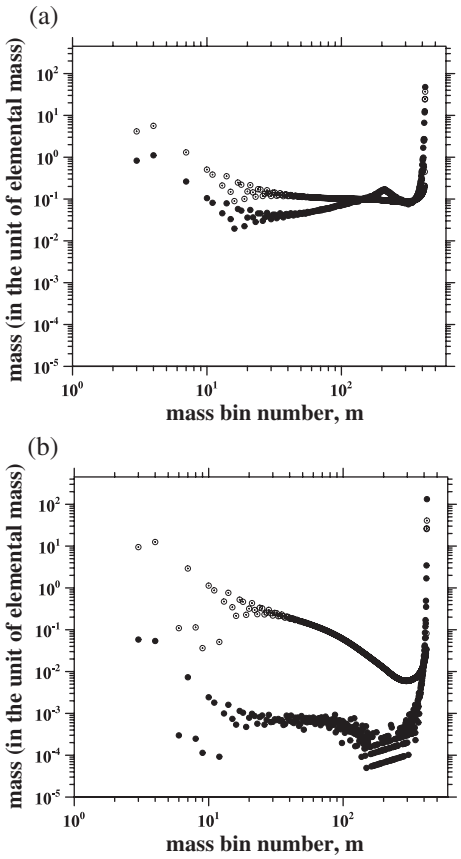


Fig. 9. Mass distributions at $t=T$ for two of the cases discussed in Section 2.1: (a) gravity kernel; (b) turbulent kernel at $\epsilon=100$ cm$^2$/s$^3$. The open circles are based on the truncated KCE and the filled circles are from Monte-Carlo simulations.

TSCE and the Monte-Carlo method to understand the stochastic correlations and fluctuations, and then apply the knowledge to design closure models for these stochastic variations when necessary.

## 4. Summary and remarks

While the potential importance of air turbulence on the collision–coalescence growth of cloud droplets has generally been recognized, quantitative descriptions of various effects of air turbulence on the collision rate are still incomplete. Turbulent coalescences of hydrodynamically interacting droplets represent a complex problem which necessarily requires sophisticated research tools. Computational approaches such as HDNS (Wang et al., 2005b) will continue to be a good quantitative research tool as they provide important data to advance the fundamental understanding of relevant physical processes. Theoretical (Zaichik et al., 2003; Zaichik and Alipchenkov, 2003) and accurate experimental tools (Shaw, 2004; Chuang and Bachalo, 2004) are also much needed, particularly when certain aspects such as the effect of flow Reynolds number may not be directly addressed by computational approaches. It is anticipated that results from DNS, theoretical, and experimental approaches will be integrated to address the Reynolds number issue in the coming years.

In this paper, we summarized our on-going efforts in quantifying the effects of turbulence and stochastic coalescence on the growth of cloud droplets. We showed that the enhanced geometric collision rates by air turbulence may reduce the time for drizzle formation due to coalescence by about 40% at $\epsilon=400$ cm$^2$/s$^3$, relative to the gravitational coalescence. Uncertainties remain on the level of droplet accumulation due to turbulence at high flow Reynolds numbers. Preliminary results also show that air turbulence can significantly increase collision efficiencies (Wang et al., 2005b). Combining these two enhancements by turbulence is

expected to further reduce the time for drizzle formation. Future work will be aimed at parameterizing these effects by combining HDNS with a theoretical approach.

We also revisited the question of stochastic completeness of the kinetic collection equation. It is shown that a true stochastic coalescence equation can be derived for arbitrary collision kernels. We also validated this new mean field equation using known analytical results and Monte-Carlo simulations. For a system of finite liquid mass and narrow initial size distribution, it is demonstrated that both stochastic correlations and fluctuations are significant. Therefore, for certain initial conditions, the stochastic correlations, which are not considered in the usual kinetic collection equation, could be another source of uncertainty in modeling rain formation. It is hoped that the TSCE will be useful in the future to improve the deterministic kinetic collection equation.

## Acknowledgments

This study has been supported by the National Science Foundation through grant ATM-0114100 and by the National Center for Atmospheric Research (NCAR). NCAR is sponsored by the National Science Foundation. Part of the computations were conducted using the IBM cluster (Bluesky) and SGI Origin 3800/2100 at NCAR.

## References

Andrews, G.E., 1998. The Theory of Partitions. Cambridge University Press, Cambridge, England.

Bayewitz, M.H., Yerushalmi, J., Katz, S., Shinnar, R., 1974. The extent of correlations in a stochastic coalescence process. J. Atmos. Sci. 31, 1604–1614.

Beard, K.V., Ochs III, H.T., 1993. Warm-rain initiation: an overview of microphysical mechanisms. J. Appl. Meteorol. 32, 608–625.

Bott, A., 1998. A flux method for the numerical solution of the stochastic collection equation. J. Atmos. Sci. 55, 2284–2293.

Brenguier, J.-L., Chaumat, L., 2001. Droplet spectra broadening in cumulus clouds. Part I: broadening in adiabatic cores. J. Atmos. Sci. 58, 628–641.

Brenguier, J.-L., Grabowski, W.W., 1993. Cumulus entrainment and cloud droplet spectra: a numerical model within a two-dimensional dynamical framework. J. Atmos. Sci. 50, 120–136.

Chaumat, L., Brenguier, J.-L., 1998. Droplet spectra broadening and concentration inhomogeneities. Proc. of the International Conf. on Cloud Physics. Amer. Meteor. Soc., Everett, WA, pp. 514–517.

Chaumat, L., Brenguier, J.-L., 2001. Droplet spectra broadening in cumulus clouds. Part II: microscale droplet concentration heterogeneities. J. Atmos. Sci. 58, 642–654.

Chuang, P., Bachalo, W., 2004. Phase-Doppler interferometry for improved cloud microphysical measurements. Proceedings of 14th International Conference on Clouds and Precipitation, Bologna, Italy, July 19–23, 2004, pp. 1056–1058.

Davila, J., Hunt, J.C.R., 2001. Settling of small particles near vortices and in turbulence. J. Fluid Mech. 440, 117–145.

de Almeida, F.C., 1979. The collisional problem of cloud droplets moving in a turbulent environment — Part II: turbulent collision efficiencies. J. Atmos. Sci. 36, 1564–1576.

Dodin, Z., Elperin, T., 2002. On the collision rate of particles in turbulent flow with gravity. Phys. Fluids 14, 2921–2924.

Franklin, C.N., Vaillancourt, P.A., Yau, M.K., Bartello, P., 2005. Collision rates of cloud droplets in turbulent flow. J. Atmos. Sci. 62, 2451–2466.

Gillespie, D., 1972. The stochastic coalescence model for cloud droplet growth. J. Atmos. Sci. 29, 1496–1510.

Gillespie, D.T., 1975a. Three models for the coalescence growth of cloud drops. J. Atmos. Sci. 32, 600–607.

Gillespie, D.T., 1975b. An exact method for numerically simulating the stochastic coalescence process in a cloud. J. Atmos. Sci. 32, 1977–1989.

Ghosh, S., Jonas, P.R., 2001. Some analytical calculations on the effect of turbulence on the settling and growth of cloud droplets. Geophys. Res. Lett. 28, 3883–3886.

Grabowski, W.W., Vaillancourt, P., 1999. Comments on "preferential concentration of clouds droplets by turbulence: effects on early evolution of cumulus cloud droplet spectra". J. Atmos. Sci. 56, 1433–1436.

Grover, S.N., Pruppacher, H.R., 1985. The effect of vertical turbulent fluctuations in the atmosphere on the collection of aerosol-particles by cloud drops. J. Atmos. Sci. 42, 2305–2318.

Hinze, J.O., 1975. Turbulence, 2nd edition. McGraw-Hill, New York, pp. 175–250.

Jameson, A.R., Kostinski, A.B., 2000. Fluctuation properties of precipitation. Part VI: observations of hyperfine clustering and drop size distribution structures in three-dimensional rain. J. Atmos. Sci. 57, 373–388.

Jeffery, C.A., 2001. Investigating the small-scale structure of clouds using the delta-correlated closure: effect of particle inertia, condensation/evaporation and intermittency. Atmos. Res. 59, 199–215 (Sp. Iss.).

Johnson, D.B., 1982. The role of giant and ultragiant aerosol particles in warm rain initiation. J. Atmos. Sci. 39, 448–460.

Jonas, P.R., 1996. Turbulence and cloud microphysics. Atmos. Res. 40, 283–306.

Khain, A., Ovtchinnikov, M., Pinsky, M., Pokrovsky, A., Krugliak, H., 2000. Notes on the state-of-the-art numerical modeling of cloud microphysics. Atmos. Res. 55, 159–224.

Klett, J.D., Davis, M.H., 1973. Theoretical collision efficiencies of cloud droplets at small Reynolds numbers. J. Atmos. Sci. 30, 107–117.

Knight, C.A., Vivekanandan, J., Lasher-Trapp, S.G., 2002. First radar echoes and the early history of Florida cumulus. J. Atmos. Sci. 59, 1454–1472.

Kogan, Y.L., 1993. Drop size separation in numerically simulated convective clouds and its effect on warm rain formation. J. Atmos. Sci. 50, 1238–1253.

Kostinski, A.B., Shaw, R.A., 2001. Scale-dependent droplet clustering in turbulent clouds. J. Fluid Mech. 434, 389–398.

Kostinski, A.B., Shaw, R.A., 2005. Fluctuations and luck in droplet growth by coalescence. Bull. Am. Meteorol. Soc. 86, 235–244.

Kruis, F.E., Kusters, K.A., 1997. The collision rate of particles in turbulent flow. Chem. Eng. Commun. 158, 201–230.

Koziol, A.S., Leighton, H.G., 1996. The effect of turbulence on the collision rates of small cloud drops. J. Atmos. Sci. 53 (13), 1910–1920.

Langmuir, I., 1948. The production of rain by a chain reaction in cumulus clouds at temperatures above freezing. J. Meteorol. 5, 175–192.

Long, A.B., 1971. Validity of the finite-difference collection equation. J. Atmos. Sci. 28, 210–218.

Maxey, M.R., 1987. The gravitational settling of aerosol-particles in homogeneous turbulence and random flow fields. J. Fluid Mech. 174, 441–465.

Pinsky, M.B., Khain, A.P., 1997. Turbulence effects on droplet growth and size distribution in clouds — a review. J. Aerosol Sci. 28, 1177–1214.

Pinsky, M.B., Khain, A.P., 2002. Fine structure of cloud droplet concentration as seen from the fast-FSSP measurements. Part II: results of in situ observations. J. Appl. Meteorol. 42, 65–73.

Pinsky, M.B., Khain, A.P., Shapiro, M., 1999. Collision of small drops in a turbulent flow. Part I. Collision efficiency. Problem formulation and preliminary results. J. Atmos. Sci. 56, 2585–2600.

Pinsky, M.B., Khain, A.P., Shapiro, M., 2000. Stochastic effects of cloud droplet hydrodynamic interaction in a turbulent flow. Atmos. Res. 53, 131–169.

Pruppacher, H.R., Klett, J.D., 1997. Microphysics of Clouds and Precipitation. Kluwer Academic Publishers, Boston. 954 pp.

Ramkrishna, D., Borwanker, J.D., 1973. A puristic analysis of population balance-I. Chem. Eng. Sci. 28, 1423–1435.

Ramkrishna, D., Borwanker, J.D., 1974. A puristic analysis of population balance-II. Chem. Eng. Sci. 29, 1711–1721.

Ramkrishna, D., Shah, B.H., Borwanker, J.D., 1976. Analysis of population balance-III. Chem. Eng. Sci. 31, 435–442.

Rogers, R.R., Yau, M.K., 1989. A Short Course in Cloud Physics. Butterworth-Heinemann, Burlington, MA. 290 pp.

Saffman, P.G., Turner, J.S., 1956. On the Collision of Drops in Turbulent Clouds. J. Fluid Mech. 1, 16–30.

Scott, W.T., 1967. Poisson statistics in distributions of coalescing droplets. J. Atmos. Sci. bf 24, 221–225.

Shaw, R.A., 2004. Particle–turbulence interactions in clouds: a measurement perspective. Proceedings of 14th International Conference on Clouds and Precipitation, July 19–23, 2004. International Conference on Clouds and Precipitation, Bologna, Italy, pp. 651–653.

Sigurgeirsson, H., Stuart, A.M., 2002. A model for preferential concentration. Phys. Fluids 14, 4352–4361.

Simmel, M., Trautmann, T., Tetzlaff, G., 2002. Numerical solution of the stochastic collection equation — comparison of the linear discrete method with other methods. Atmos. Res. 61, 135–148.

Szumowski, M.J., Rauber, R.M., Ochs, H.T., Miller, L.J., 1997. The microphysical structure and evolution of Hawaiian rainband clouds. 1: radar observations of rainbands containing high reflectivity cores. J. Atmos. Sci. 54, 369–385.

Squires, K.D., Eaton, J.K., 1990. Particle response and turbulence modification in isotropic turbulence. Phys. Fluids, A Fluid Dyn. 2, 1191–1203.

Srivastava, R.C., 1989. Growth of cloud drops by condensation: a criticism of currently accepted theory and a new approach. J. Atmos. Sci. 46, 869–887.

Su, C.-W., Krueger, S.K., McMurtry, P.A., Austin, P.H., 1998. Linear eddy modeling of droplet spectral evolution during entrainment and mixing in cumulus clouds. Atmos. Res. 47–48, 41–58.

Sundaram, S., Collins, L.R., 1997. Collision statistics in an isotropic, particle-laden turbulent suspension. J. Fluid Mech. 335, 75–109.

Telford, J.W., 1955. A new aspect of coalescence theory. J. Meteorol. 12, 436–444.

Tzivion, S., Reisin, T.G., Levin, Z., 1999. A numerical solution of the kinetic collection equation using high spectral grid solution: a proposed reference. J. Comput. Phys. 148, 527–544.

Vaillancourt, P.A., Yau, M.K., 2000. Review of particle–turbulence interactions and consequences for cloud physics. Bull. Am. Meteorol. Soc. 81, 285–298.

Vaillancourt, P.A., Yau, M.K., Grabowski, W.W., 2001. Microscopic approach to cloud droplet growth by condensation. Part I: model description and results without turbulence. J. Atmos. Sci. 58, 1945–1964.

Vaillancourt, P.A., Yau, M.K., Bartello, P., Grabowski, W.W., 2002. Microscopic approach to cloud droplet growth by condensation. Part II: turbulence, clustering, and condensational growth. J. Atmos. Sci. 59, 3421–3435.

Vohl, O., Mitra, S.K., S.C.Wurzler, H., 1999. A wind tunnel study of the effects of turbulence on the growth of cloud drops by collision and coalescence. J. Atmos. Sci. 56 (24), 4088–4099.

von Smoluchowski, M., 1917. Versuch einer mathematischen Theorie der Koagulationskinetic kolloider Losunggen. Z. Phys. Chem. 92, 129.

Wang, L.-P., Maxey, M.R., 1993. Settling velocity and concentration distribution of heavy particles in homogeneous isotropic turbulence. J. Fluid Mech. 256, 27–68.

Wang, L.-P., Wexler, A.S., Zhou, Y., 1998. Statistical mechanical descriptions of turbulent coagulation. Phys. Fluids 10, 2647–2651.

Wang, L.-P., Wexler, A.S., Zhou, Y., 2000. Statistical mechanical descriptions of turbulent coagulation of inertial particles. J. Fluid Mech. 415, 117–153.

Wang, L.-P., Ayala, O., Grabowski, W.W., 2005a. Improved formulations of the superposition method. J. Atmos. Sci. 62, 1255–1266.

Wang, L.-P., Ayala, O., Kasprzak, S.E., Grabowski, W.W., 2005b. Theoretical formulation of collision rate and collision efficiency of hydrodynamically-interacting cloud droplets in turbulent atmosphere. J. Atmos. Sci. 62, 2433–2450.

Wang, L.-P., Ayala, O. Grabowski, W.W., submitted for publication. Effects of hydrodynamic interactions on the motion of cloud droplets. J. Fluid Mech.

Warshaw, M., 1967. Cloud droplet coalescence: statistical foundations and a one-dimensional sedimentation model. J. Atmos. Sci. 24, 278–286.

Zaichik, L.I., Alipchenkov, V.M., 2003. Pair dispersion and preferential concentration of particles in isotropic turbulence. Phys. Fluids 15, 1776–1787.

Zaichik, L.I., Simonin, O., Alipchenkov, V.M., 2003. Two statistical models for predicting collision rates of inertial particles in homogeneous isotropic turbulence. Phys.Fluids 15, 2995–3005.

Zhou, Y., Wexler, A.S., Wang, L.-P., 2001. Modelling turbulent collision of bidisperse inertial particles. J. Fluid Mech. 433, 77–104.